Progress In Electromagnetics Research B, Vol. 96, 213–233, 2022

Leakage Magnetic Field Calculation and Optimization of Double Inverse Series Coil Structure of Electric Vehicle Wireless Charging Systems

Zhongqi Li[1, 2], Pengsheng Kong[1], Liquan Ren[3], Xinbo Xiong[3], Junjun Li[1, *], Wei Wu[3, *], and Huadong Liu[4]

Abstract—In the wireless power transfer (WPT) system of electric vehicles, low electromagnetic field (EMF) shielding will reduce transfer efficiency. How to reduce leakage EMF and obtain a high transfer efficiency is a difficult problem. In this paper, a double inverse series coil (DISC) structure is proposed to reduce the leakage EMF of WPT systems. First, a calculation method of EMF for rectangular coils is proposed, and the leakage EMF distribution characteristics of the coil structure on the target surface are analysed according to the proposed calculation method. Secondly, an optimization method with the optimal leakage EMF effect of the target surface is given. The parameters of each coil that meet the design requirements are obtained based on the proposed optimization method. Finally, according to the obtained coil parameters, a set of WPT system based on DISC structure is developed, and the correctness of the proposed structure and method is verified by simulated and measured results. The results show that with applying the DISC structure, the maximum leakage EMF in WPT system is only 9.56 μT on target surface without additional shielding, and the transfer efficiency is up to 95%.

1. INTRODUCTION

In recent years, wireless power transfer (WPT) has been pushed to a higher level by the rapid development of power electronics technology [1]. As a new energy transfer technology, the convenience and safety of electronic product charging have been greatly improved. This technology has been fully applied in mobile devices such as mobile phones, medical equipments, and electric vehicles [2–4]. Magnetic field is employed to exchange energy in WPT systems [5]. As the power increases, the human body will be harmed by the strong electromagnetic field (EMF) leaking into the air [6]. Therefore, it is of great significance to study the magnetic shielding method and structure of WPT systems.

In order to weaken the leakage EMF of WPT systems, passive shielding [7] and active shielding [8] are often taken into account by scholars. Passive shielding is generally used to attenuate magnetic fields in vertical direction, while active shielding is mainly aimed at the magnetic fields in horizontal direction. Ferrite and a combination shielding method of metal plates, such as copper and aluminum, are often used in passive shielding [9]. The characteristic of high magnetic permeability is utilized in the application of ferrite, while the eddy current effect is utilized in the application of metals [10]. This method not only weakens the leakage EMF in vertical direction, but also reduces the eddy current losses. In terms of ferrite applications, the loss distributions of the block core and strip core in a 5 kW wireless charging system are compared in [11]. The results show that the optimized strip core can effectively reduce the magnetic core loss by 20%. In addition, in the application of combined shielding of metal

Received 17 August 2022, Accepted 11 October 2022, Scheduled 13 October 2022
* Corresponding author: Junjun Li (862739748@qq.com), Wei Wu (antonie10@163.com).
[1] College of Railway Transportation, Hunan University of Technology, Zhuzhou 412007, China. [2] College of Electrical and Information Engineering, Hunan University, Changsha 412008, China. [3] College of Electrical and Information Engineering, Hunan University of Technology, Zhuzhou 412007, China. [4] CRRC Zhuzhou Institute Co., LTD., Zhuzhou 412007, China.

plate and ferrite, a combined shielding method of metal plate and strip core is proposed in [12]. By optimizing the radius of the metal plate and the volume of the strip core, this method reduces the eddy current loss on the one hand, and on the other hand, the strip core effectively reduces the leakage magnetic field. However, no matter whether it is a single or combined application of ferrite and metal plate, they are only aimed at the magnetic field shielding in vertical direction. There is still serious leakage of the magnetic field in horizontal direction. On the basis of passive shielding, an additional shielding coil is employed in active shielding to reduce the leakage EMF in horizontal direction.

Active shielding can be divided into independent shielding [13] and magnetic induction resonance shielding [14]. Independent shielding has independent loop compensation networks. Its reverse magnetic flux generated by applying additional reverse excitation will cancel the leakage magnetic flux from main coils. The advantage of independent shielding is that the position of the independent loop network is not restricted, so it can be set at any position in space. Therefore, in [15, 16], the independent shielding coils are placed on both sides of the main coils in horizontal and vertical directions, which reduces the leakage EMF on both sides of the main coils effectively. However, an increase of system volume and power consumption also inevitably occurs by applying the independent shielding coils. Furthermore, in order to reduce the volume of the system, the shielding coil can also be directly reversed into the main circuit of the WPT system in the design. In this situation, an excitation source is shared with the shielding coil and the main coils at the same time. A concentric shielding coil based on the circular coil is introduced in [17], and the electromagnetic simulation and measurement results show that the leakage EMF of the main coils in this structure can be effectively suppressed. However, a significant drop in transfer efficiency occurs because the main magnetic flux is weakened by the introduced concentric shielding coil. For this reason, the anti-series shielding coils are put above and below the receiving coil in [18, 19], respectively, so that the magnetic flux of the shielding coils is separated from the main flux linkage, which effectively suppresses the decline of system efficiency while achieving a low leakage EMF. The magnetic induction resonance shielding is excited by electromagnetic induction, and the current angle of the shielding coil is controlled through an external compensation capacitor to generate a reverse magnetic flux. There is no additional excitation used in this method, so the power consumption is smaller. In [20], the magnetic induction resonance shielding coil is placed vertically on sides of the main coils to reduce the influence on the main magnetic flux. However, the shielding effect is very limited, so a shielding coil is added closer to the main coils to enhance the shielding effect [21]. In addition, a double half-ring shielding coil structure has been designed in [22] for the contradictory relationship between the shielding effects and the transfer efficiency. This structure can effectively suppress the decline of the transfer efficiency while achieving a low leakage EMF, but it is hard for this method to achieve the overall magnetic shielding target in space.

In this paper, a double inverse series coil (DISC) structure is proposed to reduce the leakage EMF of WPT system. This structure is composed of two transmitting coils connected in reverse series and two receiving coils connected in reverse series too. Compared with a single set of transmitting and receiving coils, the directions of the magnetic field of two sets of transmitting and receiving coils in this structure are opposite on target surface. Due to the above characteristics, not only the system transfer efficiency is high, but also the leakage EMF of the system is weakened in this structure. Finally, the correctness of the proposed structure and method is verified by simulation and experiment. The results show that the maximum leakage EMF of WPT system is only 9.56 μT on target surface without additional shielding measures, and the transfer efficiency is up to 95%, which is significantly better than that with the conventional coil structures.

2. DISC STRUCTURE

2.1. Calculation of Magnetic Induction Intensity

In this subsection, a magnetic induction intensity calculation method for rectangular coils based on vector magnetic potential is proposed. Figure 1 shows a schematic diagram of two rectangular coils, Coil_1 and Coil_2. The length and width of Coil_1 are labeled as a_1 and a_2, and the length and width of Coil_2 are labeled as b_1 and b_2. Coil_1 can be divided into four parts (l_1, l_2, l_3, l_4), the vertical distance between o and o_1 is labeled as s_1; the current flowing in Coil_1 is labeled as the parameter I; an arbitrary

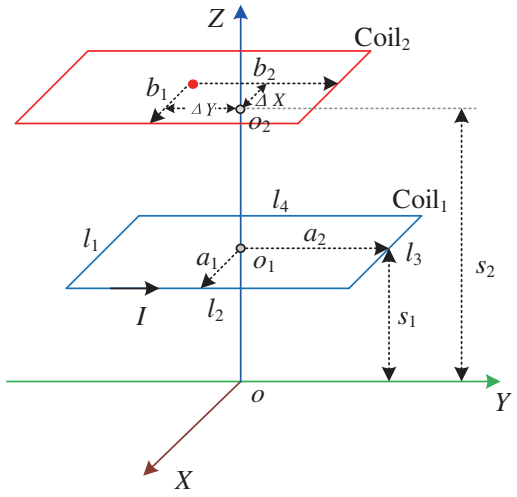

Figure 1. Schematic diagram of two rectangular coils.

point $P\ (x, y, z)$ in space is set in Figure 1, and its vector magnetic potential expression is as follows:

$$\vec{A}\,(x, y, z) = \frac{\mu_0}{4\pi} \int_v \frac{\vec{J}\,(x', y', z')\, dv'}{\vec{R}} \tag{1}$$

In Equation (1), $\vec{J}$ is the current density, v the current distribution in Coil_1, and $\vec{R}$ the distance from $P(x, y, z)$ to the source point.

$$\vec{R} = (x - x')\,\vec{e_x} + (y - y')\,\vec{e_y} + (z - z')\,\vec{e_z} \tag{2}$$

where $\vec{e_x}$, $\vec{e_y}$, and $\vec{e_z}$ represent the unit vectors of the X-axis, Y-axis, and Z-axis directions, respectively.

The double Fourier transform and its inverse transform are introduced to solve Equation (1).

$$\dot{b}\,(\xi, \eta, z) = \int_{-\infty}^{\infty} \int_{-\infty}^{\infty} B\,(x, y, z) \cdot e^{-j(x\xi + y\eta)} dxdy \tag{3}$$

$$\dot{B}\,(x, y, z) = \frac{1}{4\pi^2} \int_{-\infty}^{\infty} \int_{-\infty}^{\infty} b\,(\xi, \eta, z) \cdot e^{j(x\xi + y\eta)} d\xi d\eta \tag{4}$$

where Equation (3) represents the law of double Fourier transform, and Equation (4) represents the law of inverse transform.

Therefore, Equation (5) can be obtained by double Fourier transformation of Equation (1).

$$\begin{aligned} \vec{a}\,(\xi, \eta, z) &= \frac{\mu_0}{4\pi} \int_v \vec{J}\,(x', y', z') \cdot \left[\int_{-\infty}^{\infty} \int_{-\infty}^{\infty} \frac{1}{\vec{R}} \cdot e^{-j(x\xi + y\eta)} dxdy \right] dv' \\ &= \frac{\mu_0}{2} \int_v e^{-j(x'\xi + y'\eta)} \cdot \vec{J}\,(x', y', z') \cdot \frac{e^{-k|z - s_1|}}{k} dv' \end{aligned} \tag{5}$$

where ξ and η are double Fourier integral variables, and $k = \sqrt{\xi^2 + \eta^2}$.

The magnetic flux density $\vec{B}$ can be obtained by the vector magnetic potential $\vec{A}$.

$$\vec{B} = \nabla \times \vec{A} = \left(\frac{\partial A_z}{\partial y} - \frac{\partial A_y}{\partial z} \right) \vec{e_x} + \left(\frac{\partial A_x}{\partial z} - \frac{\partial A_z}{\partial y} \right) \vec{e_y} + \left(\frac{\partial A_y}{\partial x} - \frac{\partial A_x}{\partial y} \right) \vec{e_z} \tag{6}$$

where A_x, A_y, and A_z represent the components of the vector magnetic potential $\vec{A}$ in the X-axis, Y-axis, and Z-axis, respectively. In the same way, Equations (7), (8), and (9) can be obtained by double

Fourier transformation of Equation (6).

$$\dot{b_x} = \hat{B}_y = \left(\frac{\partial A_z}{\partial y} - \frac{\partial A_y}{\partial z}\right)^{\wedge} = -j\eta\dot{a_z} - \frac{\partial \dot{a_y}}{\partial z} \tag{7}$$

$$\dot{b_y} = \hat{B}_y = \left(\frac{\partial A_x}{\partial z} - \frac{\partial A_z}{\partial y}\right)^{\wedge} = \frac{\partial \dot{a_x}}{\partial z} + j\xi\dot{a_z} \tag{8}$$

$$\dot{b_z} = \hat{B}_z = \left(\frac{\partial A_y}{\partial x} - \frac{\partial A_x}{\partial y}\right)^{\wedge} = -j\xi\dot{a_y} + j\eta\dot{a_x} \tag{9}$$

where the symbol "$\wedge$" represents double Fourier transform.

Figure 1 shows that the component $\dot{a}_x$ of the vector magnetic potential in the X-axis can be obtained by the current parallel to the X-axis; the component $\dot{a}_y$ of the vector magnetic potential in the Y-axis can be obtained by the current parallel to the Y-axis; the component $\dot{a}_z$ is equal to zero. Equations (7), (8), and (9) can be simplified as follows:

$$\dot{b_x} = -\frac{\partial \dot{a_y}}{\partial z} \tag{10}$$

$$\dot{b_y} = \frac{\partial \dot{a_x}}{\partial z} \tag{11}$$

$$\dot{b_z} = -j\xi\dot{a_y} + j\eta\dot{a_x} \tag{12}$$

Assuming that $\dot{a}_{1x}$ is the component of the vector magnetic potential in the X-axis generated by the current of line l_1 and that $\dot{a}_{2x}$ is the component of the vector magnetic potential in the X-axis generated by the current of line l_3, we have

$$\dot{a_{1x}} = \frac{\mu_0 I \cdot e^{ja_2\eta} \cdot e^{-|z-s_1|k}}{2k} \cdot \int_{-a_1}^{a_1} e^{-jx'\xi} dx' = \frac{\mu_0 I sin\,(a_1\xi) \cdot e^{ja_2\eta} \cdot e^{-|z-s_1|k}}{\xi k} \tag{13}$$

$$\dot{a_{2x}} = \frac{\mu_0 I \cdot e^{-ja_2\eta} \cdot e^{-|z-s_1|k}}{2k} \cdot \int_{a_1}^{-a_1} e^{-jx'\xi} dx' = \frac{-\mu_0 I \sin\,(a_1\xi) \cdot e^{-ja_2\eta} \cdot e^{-|z-s_1|k}}{\xi k} \tag{14}$$

According to (13) and (14), $\dot{a}_x$ can be obtained as follows:

$$\dot{a_x} = \dot{a_{1x}} + \dot{a_{2x}} = \frac{j2\mu_0 I \sin\,(\xi a_1) \sin\,(\eta a_2) \cdot e^{-|z-s_1|k}}{\xi k} \tag{15}$$

Supposing that $\dot{a}_{1y}$ is the component of the vector magnetic potential in the Y-axis generated by the current of the line l_2 and that $\dot{a}_{2y}$ is the component of the vector magnetic potential in the Y-axis generated by the current of line l_4, we have

$$\dot{a_{1y}} = \frac{\mu_0 I \cdot e^{-ja_1\xi} \cdot e^{-|z-s_1|k}}{2k} \cdot \int_{-a_2}^{a_2} e^{-jy'\eta} dy' = \frac{\mu_0 I sin\,(a_2\eta) \cdot e^{-ja_1\xi} \cdot e^{-|z-s_1|k}}{\eta k} \tag{16}$$

$$\dot{a_{2y}} = \frac{\mu_0 I \cdot e^{ja_1\xi} \cdot e^{-|z-s_1|k}}{2k} \cdot \int_{a_2}^{-a_2} e^{-jy'\eta} dy' = \frac{-\mu_0 I sin\,(a_2\eta) \cdot e^{ja_1\xi} \cdot e^{-|z-s_1|k}}{\eta k} \tag{17}$$

According to (16) and (17), $\dot{a}_y$ can be obtained as follows:

$$\dot{a_y} = \dot{a_{1y}} + \dot{a_{2y}} = \frac{-j2\mu_0 I sin\,(\eta a_2)\, sin\,(\xi a_1) \cdot e^{-|z-s_1|k}}{\eta k} \tag{18}$$

By substituting (15) and (18) into (10), (11), and (12), we have

$$\dot{b_x} = \dot{C_x} \cdot e^{-kz} \tag{19}$$

$$\dot{b_y} = \dot{C_y} \cdot e^{-kz} \tag{20}$$

$$\dot{b_z} = \dot{C_z} \cdot e^{-kz} \tag{21}$$

where

$$\dot{C}_x = \frac{-j2\mu_0 I \sin(\xi a_1)\sin(\eta a_2)}{\eta} \cdot e^{s_1 k} \tag{22}$$

$$\dot{C}_y = \frac{-j2\mu_0 I \sin(\xi a_1)\sin(\eta a_2)}{\xi} \cdot e^{s_1 k} \tag{23}$$

$$\dot{C}_z = \frac{-2\mu_0 I k \sin(\xi a_1)\sin(\eta a_2)}{\xi\eta} \cdot e^{s_1 k} \tag{24}$$

By substituting (19), (20), and (21) into (4), the components of the magnetic flux density $\dot{B}$ in the X-axis, Y-axis, and Z-axis can be obtained by inverse double Fourier transform as follows:

$$\dot{B}_x = \frac{1}{4\pi^2}\int_{-\infty}^{\infty}\int_{-\infty}^{\infty} \dot{C}_x \cdot e^{-kz} \cdot e^{j(x\xi+y\eta)} d\xi d\eta \tag{25}$$

$$\dot{B}_y = \frac{1}{4\pi^2}\int_{-\infty}^{\infty}\int_{-\infty}^{\infty} \dot{C}_y \cdot e^{-kz} \cdot e^{j(x\xi+y\eta)} d\xi d\eta \tag{26}$$

$$\dot{B}_z = \frac{1}{4\pi^2}\int_{-\infty}^{\infty}\int_{-\infty}^{\infty} \dot{C}_z \cdot e^{-kz} \cdot e^{j(x\xi+y\eta)} d\xi d\eta \tag{27}$$

Therefore, the modulus of the magnetic flux density $\dot{B}$ can be expressed as follows:

$$B = \left|\dot{B}\right| = \sqrt{\left|\dot{B}_x\right|^2 + \left|\dot{B}_y\right|^2 + \left|\dot{B}_z\right|^2} \tag{28}$$

In addition, according to Equations (25) to (27), the mutual inductance $\dot{M}_{12}$ between Coil_1 and Coil_2 can be obtained as follows:

$$\dot{M}_{12} = \frac{1}{4\pi^2 I}\int_{-\infty}^{\infty}\int_{-\infty}^{\infty}\left(\dot{C}_z + \dot{C}_x\right) \cdot \frac{e^{j(\Delta X+b_1)\xi} - e^{j(\Delta X-b_1)\xi}}{j\xi} \cdot \frac{e^{j(\Delta Y+b_2)\eta} - e^{j(\Delta Y-b_2)\eta}}{j\eta} \cdot e^{-ks_2} d\xi d\eta \tag{29}$$

where ΔX and ΔY are the misalignments of the X-axis and Y-axis. The mutual inductance M between multiturn coils can be calculated by (30).

$$M = \left|\dot{M}\right| = \left|\sum_{m=1}^{N_1}\sum_{n=1}^{N_2} \dot{M}_{mn}\right| \tag{30}$$

where N_1 is the number of turns of Coil_1; N_2 is the number of turns of Coil_2; m is the m-th turn of Coil_1; and n is the n-th turn of Coil_2. A theoretical basis for the analysis of the leakage EMF distribution and optimization of the DISC structure is provided by the proposed magnetic field and mutual inductance calculation method in the next section.

2.2. DISC Structure

In order to obtain a lower leakage EMF and get a high transfer efficiency, a novel DISC structure is proposed to weaken the leakage EMF of WPT on target surface. The advantage of the proposed structure is low leakage EMF and high transfer efficiency. The receiving side of the structure is composed of two anti-series coils R_{x1} and R_{x2}, and the transmitting side is composed of two anti-series coils T_{x1} and T_{x2}. T_{x1} and R_{x1} are coaxial, and T_{x2} and R_{x2} are also coaxial, as shown in Figure 2.

According to the coil structure in Figure 2, an equivalent circuit model can be obtained, as shown in Figure 3.

Parameters L_1 and L_2 are defined as self-inductances of the transmitting coil and receiving coil, and R_1 and R_2 are defined as internal resistances of the transmitting coil and receiving coil. C_{Tx} and C_{Rx} are defined as the resonance capacitances of the transmitting and receiving coils. M is defined as the mutual inductance between the coils, and R_s is defined as the internal resistance of the power supply $\dot{V}_s$. According to Figure 3, the Kirchhoff voltage equation matrix can be obtained as:

$$\begin{bmatrix} \dot{Z}_1 & j\omega M \\ j\omega M & \dot{Z}_2 \end{bmatrix} \begin{bmatrix} \dot{I}_{Tx} \\ \dot{I}_{Rx} \end{bmatrix} = \begin{bmatrix} \dot{V}_S \\ 0 \end{bmatrix} \tag{31}$$

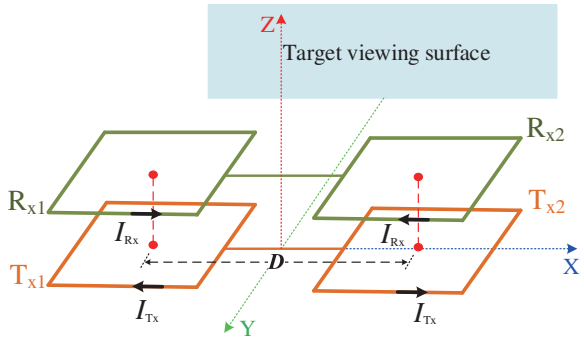

Figure 2. Schematic diagram of the proposed coil structure.

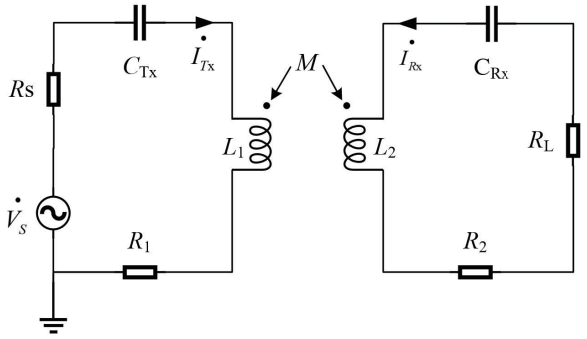

Figure 3. Schematic diagram of the equivalent circuit.

The currents of transmitting and receiving coils can be solved as:

$$\begin{cases} \dot{I_{Tx}} = \dfrac{\dot{Z}_2 \dot{V}_S}{\dot{Z}_1 \dot{Z}_2 + (\omega M)^2} \\ \dot{I_{Rx}} = -\dfrac{j\omega M \dot{V}_S}{\dot{Z}_1 \dot{Z}_2 + (\omega M)^2} \end{cases} \tag{32}$$

where $\dot{Z}_1$ and $\dot{Z}_2$ represent the impedances of the transmitting and receiving coils, and their expressions are as follows:

$$\begin{cases} \dot{Z}_1 = R_s + R_1 + j\omega L_1 - j\dfrac{1}{\omega C_{Tx}} \\ \dot{Z}_2 = R_2 + R_L + j\omega L_2 - j\dfrac{1}{\omega C_{Rx}} \end{cases} \tag{33}$$

According to the current expression, the system transfer efficiency η can be further obtained.

$$\eta = \left| \frac{\dot{I}_{Rx}^2 R_L}{\dot{V}_S \dot{I}_{Tx}} \right| = \left| -\frac{(\omega M)^2 R_L}{\dot{Z}_1 \dot{Z}_2^2 + (\omega M)^2 \dot{Z}_2} \right| \tag{34}$$

When the system works in the resonance state, there are: Z_1=R_s+R_1, Z_2=R_2+R_L, and the new efficiency expression can be further obtained.

$$\eta = \frac{(\omega M)^2 R_L}{(R_s + R_1)(R_2 + R_L)^2 + (\omega M)^2 (R_2 + R_L)} \tag{35}$$

By the derivation of R_L, the optimal load R_{Lopt} can be obtained when the efficiency is maximum, and its expression is:

$$R_{Lopt} = \sqrt{\frac{(R_s + R_1) R_2^2 + (\omega M)^2 R_2}{(R_s + R_1)}} \tag{36}$$

It can be seen from Equation (37) that the optimal load R_{Lopt} is not only related to the internal resistance of the coil, but also related to the mutual inductance of the coil. In order to further improve the transfer efficiency of the system, the mutual inductance under the misalignment of 15 cm between transmitting and receiving coils should be used to calculate the optimal load.

In terms of weakening leakage EMF, the leakage EMF distribution on the target viewing surface is closely related to the series connection direction of the coils. Figure 4 shows a schematic diagram of the EMF distribution when the coils are connected in series in different directions. Figure 4(a) is the EMF distribution when the coils are connected in the forward series connection. Figure 4(b) is the EMF distribution when the coils are connected in the reverse series connection. It is not difficult to see that when being connected in series in the forward direction, the magnetic fields of T_{x1}-R_{x1} and T_{x2}-R_{x2} are superimposed in the same direction, and the total magnetic flux density B_{total} is greatly enhanced. On the contrary, when the reverse series is used, the EMFs of T_{x1}-R_{x1} and T_{x2}-R_{x2} are opposite at any point on the target viewing surface, which leads to greatly weakened B_{total} of the system.

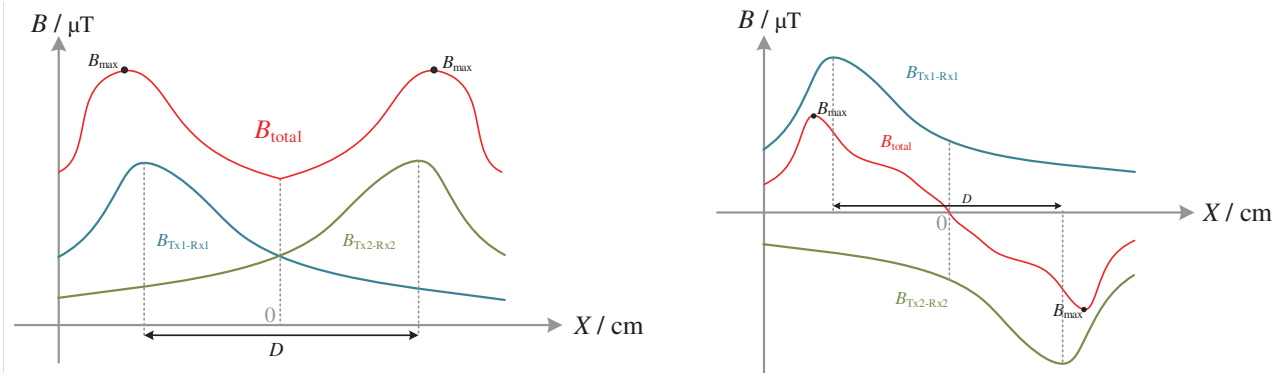

(a) Magnetic field distribution in co-direction series

(b) Magnetic field distribution in reverse series

Figure 4. Magnetic field distribution at the target viewing surface.

Besides, in order to illustrate the principle of magnetic field weakening more intuitively, a schematic diagram of the superposition of magnetic field vectors is introduced, as shown in Figure 5. The magnetic field vector of the transmitting coil T_{x1} is represented as B_{Tx1}, and the magnetic field vector of the transmitting coil T_{x2} is represented as B_{Tx2}. Since T_{x1} and T_{x2} are connected in reverse series, B_{Tx1} and B_{Tx2} are reversed. Similarly, the receiving coils R_{x1} and R_{x2} are connected in reverse series so that their respective magnetic field vectors B_{Rx1} and B_{Rx2} are also reversed. Finally, the synthetic magnetic field B_{WPT1} of T_{x1}-R_{x1} is opposite to the synthetic magnetic field B_{WPT2} of T_{x2}-R_{x2}. The total magnetic field B_{total} at any point on the target viewing surface is lower than the leakage magnetic field of a single set of transmitting and receiving coils.

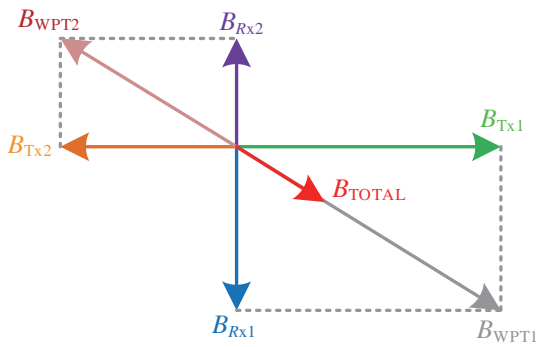

Figure 5. Diagram of the superposition of magnetic field vectors.

2.3. Characteristics of Leakage EMF Distribution

In electric vehicle applications, the transmitting and receiving coils are typically placed in the center of the parking space, respectively. According to the fourth part of the GB/T.38775 [23], the area around the vehicle that can be reached by the human body is divided into two parts, namely the protection areas $3a$ and $3b$ in Figure 6. According to Biosafar's law, the magnetic field is inversely proportional to the distance from any point in space to the coil. Therefore, the maximum leakage magnetic field point should be found in the protection area $3a$ because it is closer to the coils. Since the width of the vehicle chassis is generally about 1600 mm, the maximum leakage magnetic field point can be found on the observation surface 800 mm away from the center of the vehicle chassis.

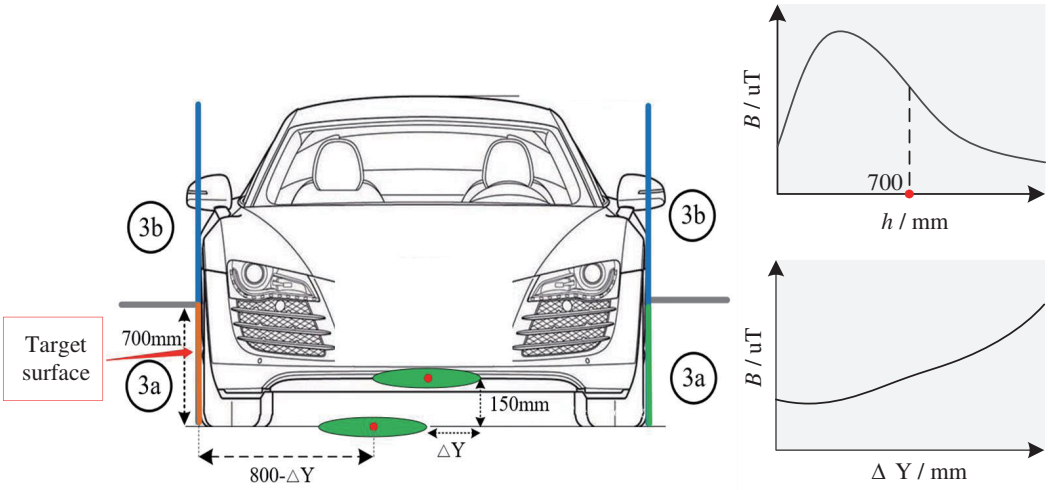

Figure 6. Schematic diagram of the leakage magnetic field viewing surface.

In addition, when the electric vehicle chassis is misaligned, the leakage magnetic field on the vehicle edge will be significantly enhanced as the misalignment distance ΔY increases. Therefore, the maximum leakage magnetic field point should also be found in extreme misalignment of 15 cm in this paper.

2.4. Leakage EMF Optimization

In this subsection, according to the proposed formula for calculating the magnetic field of rectangular coils, the parameters of the DISC structure are optimized to achieve a safe leakage magnetic field. The flowchart of the leakage magnetic field optimization method is shown in Figure 7.

According to Equations (1) to (28), the magnetic induction intensity is related to the length, width, and relative position of the rectangular coil. When the misalignment distance between transmitting and receiving coils is within 15 cm, the parameters of each coil (such as length, width, number of turns, etc.) can be optimized to maintain the maximum leakage magnetic field of the target viewing surface below the safe value of 27 μT [24]. The specific steps of the optimization method are as follows:

(1) Parameters setting and initialization: The transfer distance between transmitting and receiving coils is set to 15 cm. The conductors are made of copper wire with a diameter of 3.9 mm. The maximum leakage magnetic field $B_{\max}$ is set to 27 μT. The output power P is set to 10 kW.

(2) Set constraints: Set constraints according to the actual situation. In this paper, T_{x1} and T_{x2}, R_{x1} and R_{x2} have the same dimensions, and the inner lengths of $T_{x1}(l_1)$ and $T_{x2}(l_2)$ are changed from 20 to 25 cm. The inner lengths of $R_{x1}(l_3)$ and $R_{x2}(l_4)$ are changed from 25 to 30 cm. The numbers of turns for $T_{x1}(N_1)$ and $T_{x2}(N_2)$ are changed from 20 to 30. The numbers of turns for $R_{x1}(N_3)$ and $R_{x2}(N_4)$ are changed from 10 to 20. The step of the number of turns is 1 turn. The change of inner length is 1 cm. The larger the range of inner lengths is, the more results there are. However, the larger the range of inner lengths is, the correspondingly longer the computation time is. Therefore,

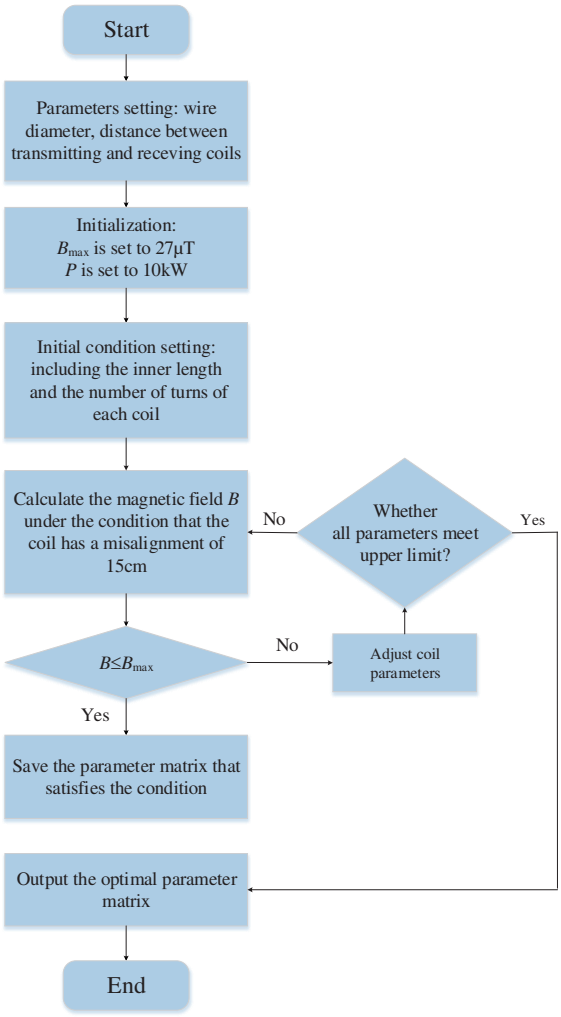

Figure 7. Flow chart of leakage EMF optimization method.

it is important to select the appropriate range of inner lengths according to the needs of the actual application.

(3) Calculate leakage magnetic field B: The X-axis range is $(-100, 100)$ cm; the Z-axis range is $(0, 70)$ cm; and the Y-axis is set to $(-65, 80)$ cm. According to Equations (1) to (29), the distribution of leakage magnetic field on the target viewing surface under misalignment can be calculated; the maximum leakage magnetic field is obtained; and the coordinates of this point are determined.

(4) Conditional judgment: In order to keep the magnetic field level to be safe, the condition $B \leq 27\,\mu$T must be satisfied. If the result meets the above condition, the result will be saved. Otherwise, the result will not be saved, and the coil parameters will continue to be optimized. If all coil parameters reach the maximum value, the optimization program of leakage magnetic field is ended; otherwise, the procedure jumps to step (3).

(5) Output the found solutions: Results that satisfy all setting conditions are saved and outputted.

3. EXPERIMENT VERIFICATION

3.1. Experimental Setup

According to the parameters of optimization method, the parameters of the coils that meet the conditions are obtained. The parameters of the coils are shown in Table 1 in detail. The physical

Table 1. Parameters of coils.

Coils	Turns	Inner length/cm	Outside length/cm
T_{x1}	25	23	42
T_{x2}	25	23	42
R_{x1}	15	27	38
R_{x2}	15	27	38

parameters of the coils are shown in Table 2 in detail. According to the parameters in Table 1, a DISC structure physical model is developed. All coils are wound with Litz wire to reduce the internal resistance. The Litz wire specification of all coils is $\phi 0.1m \times 800$ strands, and the maximum withstand current is 31.415 A. As shown in Figure 8(a), the prototype model of the system includes a transmitting coil T_x and a receiving coil R_x, wherein the transmitting coil T_x is composed of two identical coils T_{x1} and T_{x2} in anti-series, as shown in Figure 8(b). The receiving coil R_x is composed of two identical coils R_{x1} and R_{x2} in anti-series, as shown in Figure 8(c). In addition, the NF-5035s electromagnetic radiation analyzer is used to measure the magnetic field; the WT-5000 power analyzer is used to measure the real-time transfer efficiency of the system; and the inverter module and rectifier module use SiC power devices with model C3M0075120D. The maximum rated current of the power device can reach up to 30 A, which can meet the requirements of the experiment. The calculated, simulated, and measured

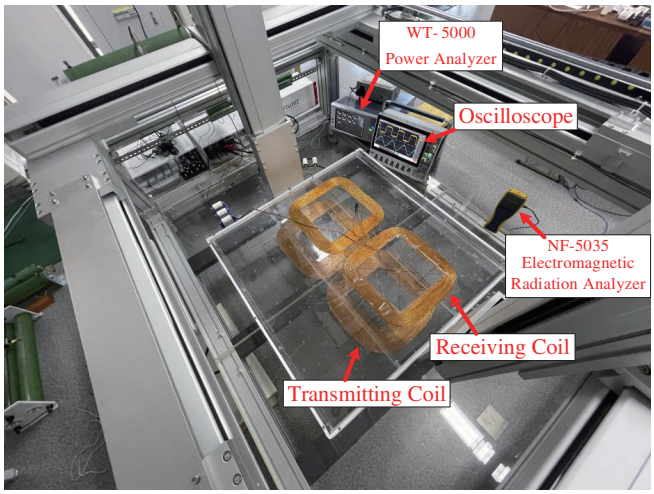

(a) Overall experimental map

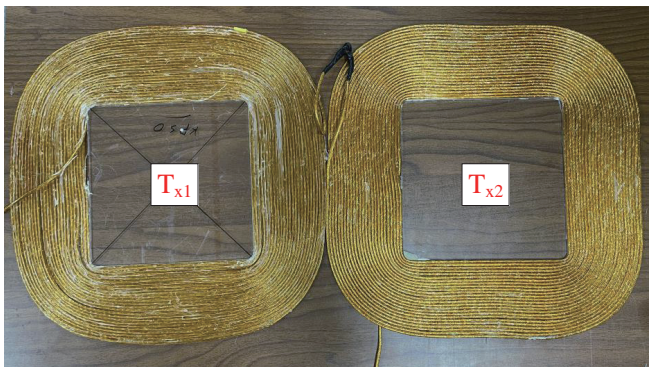

(b) Transmitting Coil

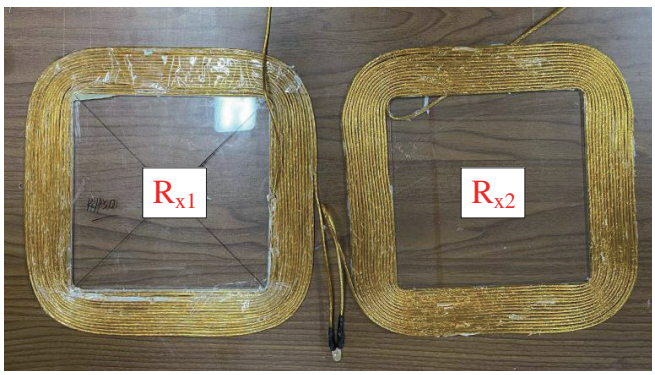

(c) Receiving Coil

Figure 8. Experimental setup.

Table 2. Measurement parameters of the DISC structure.

Parameter	Physical meaning	Value
$L_1/\mu H$	Self-inductance of transmitting coil	680
$L_1/\mu H$	Self-inductance of receiving coil	291
C_{Tx}/nF	Compensation capacitance of transmitting coil	5.2
C_{Rx}/nF	Compensation capacitance of receiving coil	12.1
$R_1/m\Omega$	Parasitic resistance of transmitting coil	560
$R_2/m\Omega$	Parasitic resistance of receiving coil	205
f_0/kHz	Working frequency	85
R_L/Ω	Load	25

Table 3. Calculated value M_c, simulated value M_s, and measured value M_e of mutual inductance with misalignments along the Y-axis in the proposed DISC structure.

Misalignment/cm	$Mc/\mu H$	$Ms/\mu H$	$Me/\mu H$
0	88.23	90.13	92.65
3	86.85	88.35	91.23
6	82.37	82.01	86.75
9	76.85	74.23	80.75
12	69.03	69.10	71.50
15	60.11	63.25	61.25

values of the mutual inductance with misalignments along the Y-axis are shown in Table 3, where the calculated value is obtained from Equation (30), the simulated value obtained from Ansys Maxwell, and the measured value is measured by IM3536 impedance analyzer.

3.2. Leakage EMF of Proposed Structure

In order to analyze the leakage magnetic field of the proposed novel DISC structure, according to Equations (1) to (28), the three-dimensional leakage EMF of the target viewing surface with a maximum misalignment of 15 cm along the Y-axis is calculated first with the help of matlab when the system transmission power is set to 10 kW. The coordinates corresponding to the maximum calculated leakage EMF B_c are found according to the calculated results of EMF. As shown in Figure 9, the maximum calculated leakage EMF is only 9.96 μT when the DISC structure is applied. The coordinates of the maximum leakage magnetic field point may be taken as $(-330, -800 + \Delta Y, 200)$ mm.

Then, the DISC structure model is drawn by Ansys Maxwell, as shown in Figure 10, and the simulated leakage magnetic field B_s at the maximum leakage magnetic field point is obtained by using the simulation model. Finally, the measured leakage magnetic field B_e at the maximum leakage magnetic field point of the target viewing surface under the DISC structure is obtained by NF-5035s electromagnetic radiation analyzer. The error between the simulated and the calculated results is defined as ε_s, and the error between the measured and calculated results is defined as ε_e. The two expressions are:

$$\varepsilon_s = \frac{|B_c - B_s|}{B_s} \times 100 \tag{37}$$

$$\varepsilon_e = \frac{|B_c - B_e|}{B_e} \times 100 \tag{38}$$

Table 4 shows the calculated, simulated, measured values of magnetic field and error rates of the magnetic field with misalignments along the Y-axis under the DISC structure. It can be seen from

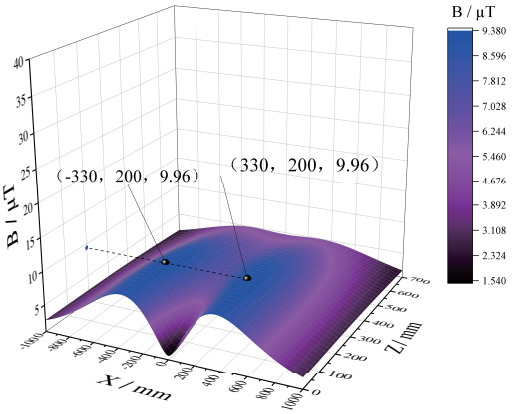

Figure 9. Three-dimensional distribution of calculated leakage EMF on the target viewing surface.

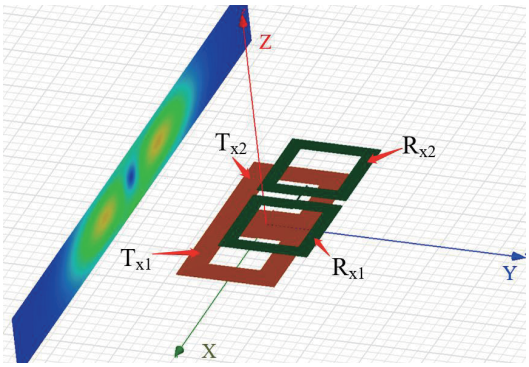

Figure 10. Simulation model of the DISC structure.

Table 4. Calculated, simulated, measured values of magnetic field and error rates with misalignments along the Y-axis in the proposed DISC structure.

Misaligment/cm	***Bc*/μT**	***Bs*/μT**	***Be*/μT**	ε_s/%	ε_e/%
0	3.87	4.06	4.04	4.7	4.2
3	4.27	4.21	4.41	1.4	3.2
6	4.92	5.11	5.15	3.7	4.5
9	5.89	6.15	6.19	4.2	4.8
12	7.46	7.78	7.56	4.1	1.3
15	9.96	9.72	9.56	2.5	4.2

Table 4 that the maximum error ε_s is 4.7%, and the maximum error ε_e is 4.8%. In addition, the measured maximum leakage magnetic field is only 9.56 μT at the maximum misalignment of 15 cm, which is far below the safe value of 27 μT. This proves that the DISC structure has the advantage of low leakage magnetic field.

The change of maximum leakage EMF at the target surface when the system is misaligned along the X-axis is shown in Table 5. It can be seen from Table 5 that the maximum error ε_s is 4.8%, and the maximum error ε_e is 4.2%. The measured maximum leakage EMF is 6.11 μT at the maximum misalignment of 15 cm along the X-axis, which is smaller than the maximum leakage EMF under the maximum misalignment of 15 cm along the Y-axis. It indicates that the leakage EMF of the target

Table 5. Calculated, simulated, measured values of magnetic field and error rates with misalignments along the X-axis in the proposed DISC structure.

Misalignment/cm	$Bc/\mu T$	$Bs/\mu T$	$Be/\mu T$	$\varepsilon_s/\%$	$\varepsilon_e/\%$
0	3.87	4.06	4.04	4.7	4.2
3	4.19	4.12	4.15	1.7	1.0
6	4.35	4.57	4.34	4.8	0.2
9	4.62	4.81	4.72	3.9	2.1
12	5.11	5.22	5.23	2.1	2.3
15	6.01	5.82	6.11	3.2	1.6

surface under the DISC structure is maximum in the condition of the maximum misalignment along the Y-axis.

According to the data in Table 4 and Table 5, the variation curve of leakage EMF with misalignments is shown in Figure 11. It is not difficult to see from Figure 11 that the leakage magnetic field increases with the increase of the misalignment between the transmitting and receiving coils, and the increase of the leakage magnetic field with misalignments along the Y-axis is more obvious than that along the X-axis. This is because the target surface will move with the misalignment of the receiving coil along the Y-axis, but will not move with the misalignment of the receiving coil along the X-axis. The calculated, simulated, and measured leakage magnetic fields are in good agreement at all misalignments, which verifies the effectiveness of the proposed structure and method.

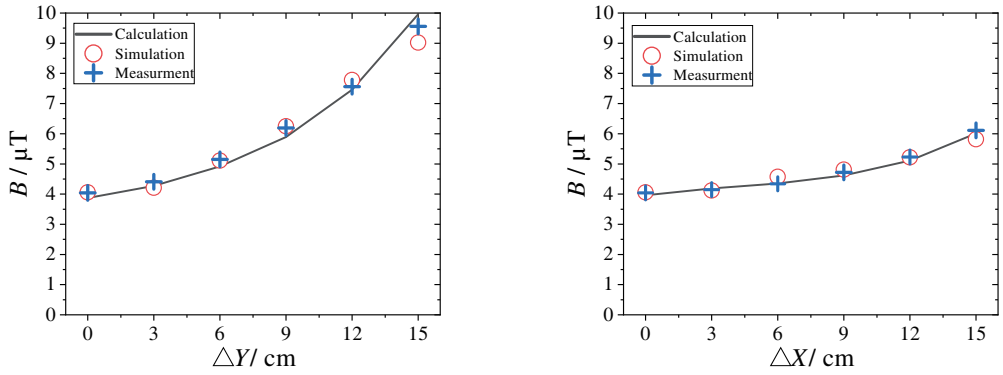

(a) Misalignment along with Y-axis

(b) Misalignment along with X-axis

Figure 11. Leakage EMF versus misalignments under the DISC structure.

3.3. Leakage Magnetic Fields of Conventional Coil Structures

In order to show the superiority of the proposed DISC structure, first the three-dimensional calculated leakage EMF under the conventional coil structure is compared with the three-dimensional calculated leakage EMF of the target surface under the DISC structure. The three-dimensional calculated leakage EMF is obtained when a single set of conventional coils T_{x1}-R_{x1} provides a power that is the same as the DISC structure to the load with a maximum misalignment of 15 cm along the Y-axis. As shown in Figure 12, when using the conventional coil structure, the calculated leakage EMF B_c of the target surface is concentrated in the local area which is closer to the coils. The coordinates of the maximum leakage EMF point are (0, −650, 0) mm, and the corresponding maximum leakage EMF is 39.33 μT which is far beyond the safe limit of 27 μT.

Then, the conventional coil model is drawn by Ansys Maxwell, as shown in Figure 13, and the simulated leakage magnetic field B_s at the point of maximum leakage magnetic field is obtained by

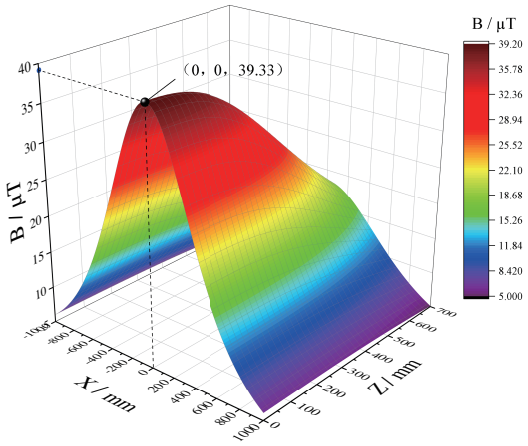

Figure 12. Three-dimensional calculated leakage EMF distribution of the target surface under the conventional coil.

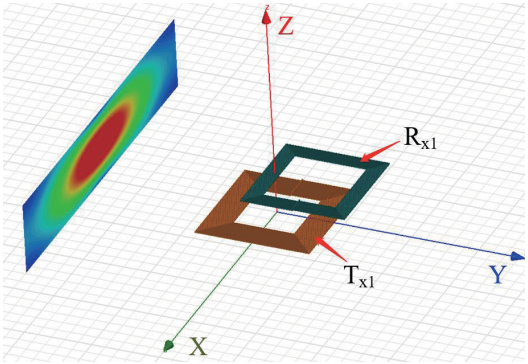

Figure 13. Simulation model of conventional coil structure.

using the simulation model. Finally, the measured leakage magnetic field B_e of the conventional coil structure is achieved by NF-5035s electromagnetic radiation analyzer.

The calculated, simulated, measured values of magnetic field and error rates of the magnetic field with misalignments along the Y-axis are shown in Table 6. It can be seen from Table 6 that the maximum error ε_s is 3.1%, and the maximum error ε_e is 4.6%. In addition, with an increase of misalignment, the measured maximum leakage EMF of the target surface is enhanced from 14.86 μT to 40.93 μT, which is increased by 26.07 μT. Obviously, for the conventional coil structure, the leakage EMF will cause harm to the human body if no additional shielding measures are applied.

Table 6. Calculated, simulated, measured values of magnetic field, and error rates with misalignments along the Y-axis in the conventional coil structure.

Misalignment/cm	$\boldsymbol{Bc}/\mu$**T**	$\boldsymbol{Bs}/\mu$**T**	$\boldsymbol{Be}/\mu$**T**	$\varepsilon_s/\%$	$\varepsilon_e/\%$
0	14.40	14.75	14.86	2.4	3.1
3	16.09	16.61	16.83	3.1	4.4
6	18.82	19.32	19.53	2.6	3.6
9	22.92	23.56	24.03	2.7	4.6
12	29.33	28.53	30.14	2.8	2.7
15	39.33	40.26	40.93	2.3	3.9

Table 7. Calculated, simulated, measured values of magnetic field and error rates with misalignments along the X-axis in the conventional coil structure.

Misalignment/cm	$Bc/\mu T$	$Bs/\mu T$	$Be/\mu T$	$\varepsilon_s/\%$	$\varepsilon_e/\%$
0	14.40	13.95	14.86	3.2	3.1
3	14.60	15.12	15.07	3.4	3.1
6	15.28	15.76	16.01	3.0	4.6
9	16.41	15.83	17.22	3.7	4.7
12	18.26	18.91	18.77	3.4	2.7
15	21.03	22.01	21.92	4.4	4.2

Table 7 shows the maximum leakage EMF variations of the target surface when the system is misaligned along the X-axis. It can be seen from Table 7 that the maximum error ε_s is 4.4%, and the maximum error ε_e is 4.7%. The measured maximum leakage EMF is 21.92 μT at the maximum misalignment of 15 cm along the X-axis, which is smaller than the measured maximum leakage EMF at the maximum misalignment of 15 cm along the Y-axis. However, no matter whether the system is misaligned along the X-axis or Y-axis, the leakage magnetic field with traditional coils is far beyond the leakage magnetic field of the DISC structure.

Besides, in order to facilitate the observation of the change trend, according to the data in Table 6 and Table 7, the change curve of the leakage EMF with the misalignment is drawn, as shown in Figure 14. It can be seen from Figure 14 that the increase of leakage EMF with misalignments along the Y-axis is more obvious than that along the X-axis. This is because the coil current increases when the system misaligns along the X-axis, and the relative position of the target surface and transmitting coil remains unchanged. When the system misaligns along the Y-axis, not only the coil current increases, but also the distance between the target surface and the transmitting coil is closer. At the misalignment of 15 cm, the leakage EMF along the Y-axis is 76% higher than that of the proposed DISC structure, and the leakage EMF along the X-axis is 72% higher than that of the proposed DISC structure.

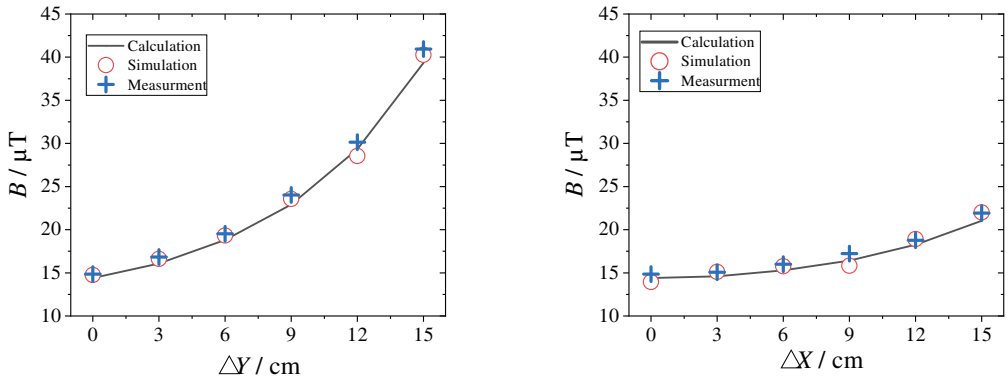

(a) Misalignment along with Y-axis (b) Misalignment along with X-axis

Figure 14. Leakage EMF versus misalignments under the conventional coil structure.

3.4. Leakage Magnetic Fields of Co-Direction Series Coil Structure

In order to verify the principle of magnetic shielding in Figure 4, the theoretical value of the leakage magnetic field under the co-direction series coil structure is further compared with the theoretical value of the leakage magnetic field of the DISC structure. When the co-direction series coil structure is used, the three-dimensional leakage EMF B_c of the target surface with a maximum misalignment of 15 cm along the Y-axis is calculated with the help of Matlab, as shown in Figure 15. The coordinates of the

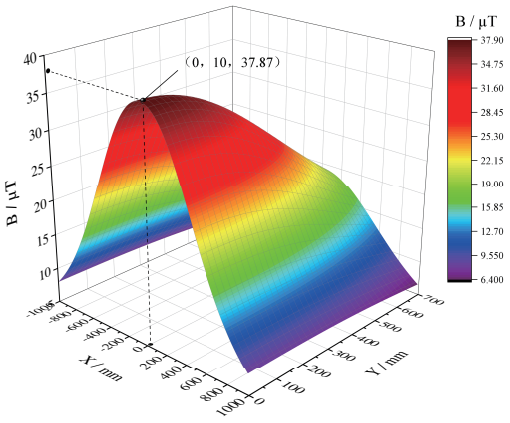

Figure 15. Three-dimensional calculated leakage EMF distribution of the target surface under the co-direction series coil structure.

maximum leakage EMF point are (0, −650, 10) mm, and the corresponding maximum leakage EMF is 37.87 μT which is close to the maximum leakage EMF of the conventional coil structure. This is because when using the co-direction series coil structure, the components of the magnetic flux density on the X-axis cancel each other, and the magnetic flux density components on the Y-axis and Z-axis are superimposed. Besides, when the distance D between two sets of transmitting and receiving coils in Figure 4 is small enough, the two maximum leakage magnetic field points will be superposed into one. However, the maximum leakage EMF of the superposition also far exceeds that of the DISC structure.

Then, the co-direction series coil model is drawn by Ansys Maxwell, as shown in Figure 16, and the simulated leakage magnetic field B_s at the point of maximum leakage magnetic field is obtained by using the simulation model. Finally, the measured leakage magnetic field B_e of the co-direction series coil structure is obtained by NF-5035s electromagnetic radiation analyzer.

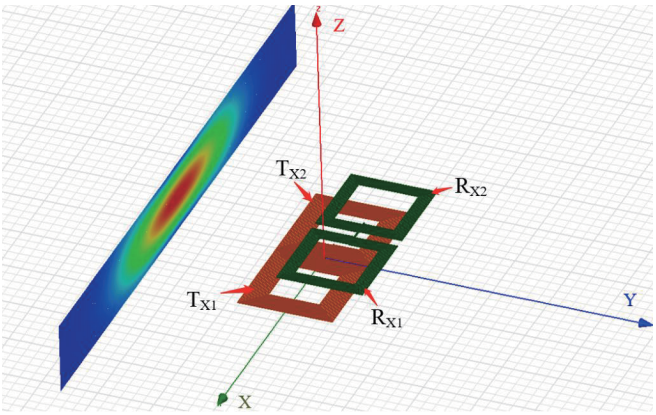

Figure 16. Simulation model of co-direction series coil structure.

The calculated, simulated, measured values of magnetic field and error rates with misalignments along the Y-axis are shown in Table 8. It can be seen from Table 8 that the maximum error ε_s is 4.9%, and the maximum error ε_e is 4.2%. With an increase in misalignment, the measured maximum leakage EMF of the target surface is enhanced from 17.71 μT to 39.32 μT, which is increased by 21.61 μT. This means that the co-direction series coil structure also requires additional magnetic shielding measures.

Table 9 shows the calculated, simulated, measured values of magnetic field and error rates with misalignments along the X-axis. It can be seen from Table 9 that the maximum error ε_s is 4.7%, and the maximum error ε_e is 4.2%. The measured maximum leakage EMF is 20.79 μT with the

Table 8. Calculated, simulated, measured value of magnetic field, and error rates with misalignments along the Y-axis in the co-direction series coil structure.

Misalignment/cm	$Bc/\mu T$	$Bs/\mu T$	$Be/\mu T$	$\varepsilon_s/\%$	$\varepsilon_e/\%$
0	16.96	17.64	17.71	3.9	4.2
3	18.20	17.35	18.90	4.9	3.7
6	20.30	20.69	21.04	1.9	3.5
9	23.65	23.99	23.21	1.4	1.9
12	29.03	28.72	30.11	1.1	3.6
15	37.87	38.04	39.32	0.4	3.7

Table 9. Calculated, simulated, measured value of magnetic field, and error rates with misalignments along the X-axis in the co-direction series coil structure.

Misalignment/cm	$Bc/\mu T$	$Bs/\mu T$	$Be/\mu T$	$\varepsilon_s/\%$	$\varepsilon_e/\%$
0	16.96	17.64	17.71	3.9	4.2
3	17.10	17.82	17.50	4.0	2.3
6	17.49	17.66	17.99	1.0	2.8
9	18.12	18.34	18.92	1.2	4.2
12	18.96	19.26	19.45	1.6	2.5
15	20.02	21.01	20.79	4.7	3.7

misalignment of 15 cm along the X-axis, which is smaller than the measured maximum leakage EMF with the misalignment of 15 cm along the Y-axis. Therefore, the leakage EMF of the co-direction series coil structure and traditional coil structure are very close at a misalignment of 15 cm along the X-axis and Y-axis, which further illustrates the low leakage EMF of the proposed DISC structure.

In order to show the tendency of the change, according to the data in Table 8 and Table 9, the change curve of the leakage EMF with the misalignment is drawn, as shown in Figure 17. It can be seen from Figure 17 that the increase of leakage EMF with misalignments along the Y-axis is higher than that along the X-axis. At the misalignment of 15 cm, the leakage EMF along the Y-axis is 74% higher than that of the proposed DISC structure, and the leakage EMF along the X-axis is 72% higher than that of the proposed DISC structure.

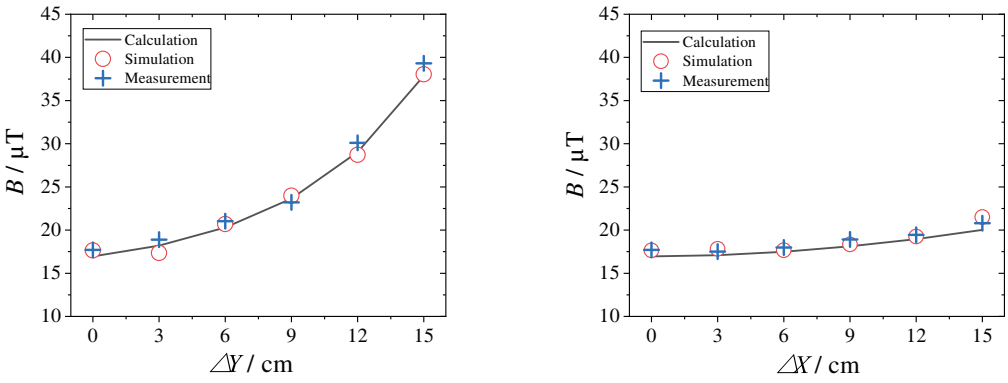

(a) Misalignment along with Y-axis (b) Misalignment along with X-axis

Figure 17. Leakage EMF versus misalignments under the co-direction series coil structure.

3.5. Transfer Efficiency of DISC Structure

In order to analyze the change of the system transfer efficiency, the calculated value η_c of the system transfer efficiency is first obtained through Equations (31) to (35). Secondly, the simulated value η_s is obtained by Matlab/Simulink. Finally, the measured value η_e is obtained by the WT-5000 power analyzer.

Table 10 shows the system transfer efficiency with misalignments along the Y-axis. It is not difficult to see from Table 10 that the measured maximum transfer efficiency is the largest when the coil is coaxial, which reaches up to 98.57%. As the misalignment increases, the system transfer efficiency reaches the minimum at the maximum misalignment of 15 cm. The measured minimum transfer efficiency is 95%, which is lower than the calculated minimum transfer efficiency. This is because the simulated internal resistance of the coil is used to calculate the theoretical transfer efficiency, and the simulated internal resistance is about twice smaller than the measured internal resistance, so the measured transfer efficiency is greatly reduced.

Table 10. Caculated, simulated, and measured values of transfer efficiency with misalignments along the Y-axis.

Misaligment/cm	$\eta_c/\%$	$\eta_s/\%$	$\eta_e/\%$
0	99.14	97.79	98.57
3	99.13	97.77	97.88
6	99.10	97.74	97.42
9	99.04	97.59	96.75
12	98.95	97.45	95.52
15	98.79	97.35	95.00

Table 11 shows the transfer efficiency with misalignments along the X-axis. The measured transfer efficiency at the maximum misalignment of 15 cm is 94.78%, which is smaller than the calculated transfer efficiency at the maximum misalignment of 15 cm. This shows that the structure proposed in this paper not only has the advantages of low leakage EMF, but also has strong ability of anti-migration.

Table 11. Caculated, simulated, and measured values of transfer efficiency with misalignments along the X-axis.

Misaligment/cm	$\eta_c/\%$	$\eta_s/\%$	$\eta_e/\%$
0	99.14	97.78	98.57
3	99.13	97.77	97.80
6	99.11	97.73	97.37
9	99.07	97.47	96.31
12	99.02	97.20	95.33
15	98.96	96.82	94.78

Finally, according to the data in Table 10 and Table 11, the change curve of the transfer efficiency with the misalignment is drawn, and the change of the system transfer efficiency can be seen more intuitively, as shown in Figure 18. It can be seen that the system transfer efficiency decreases with the increase of misalignment. This is because the mutual inductance decreases due to misalignment. When the misalignment is within 15 cm, the change in transfer efficiency is very small when the system is misaligned along the X-axis and Y-axis, and the measured minimum transfer efficiency remains about 95%.

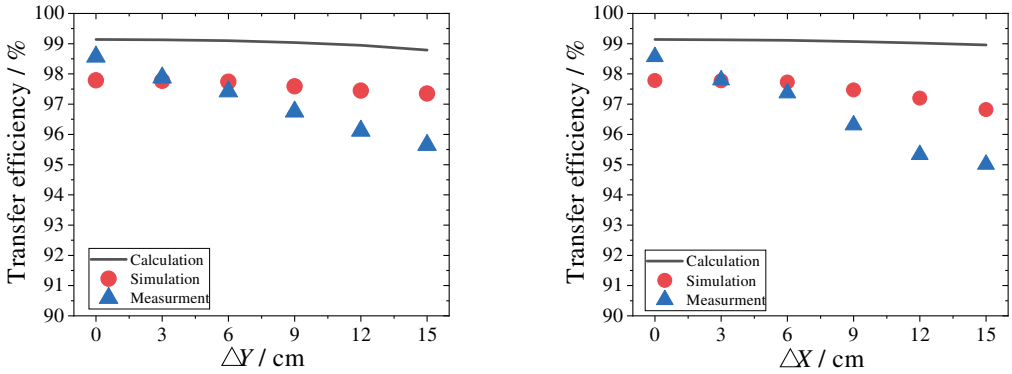

(a) Misalignment along with Y-axis

(b) Misalignment along with X-axis

Figure 18. Transfer efficiency versus misalignments.

4. CONCLUSION

This paper proposes a double inverse series coil structure. The main feature of this structure is that the magnetic fields of the two sets of transmitting and receiving coils are opposite on the target surface. This feature provides a theoretical basis for improving the transfer efficiency and the leakage magnetic field of the system. In addition, an optimization method of coil parameters is also proposed. Through the proposed optimization method, the optimal parameters of each coil can be obtained. Then, the safe leakage magnetic field under the target system power is obtained by using the optimal parameters. Not only are the proposed structure and optimization method simple, but also the system can achieve a safe leakage EMF of 9.56 µT within a misalignment of 15 cm, and the transfer efficiency can still be maintained at about 95%. The calculated, simulated, and measured results show that compared with the conventional coil structures, the novel coil structure reduces the leakage EMF by about 77% at the same transmission power, which greatly improves the safety of the electromagnetic environment around the electric vehicles during charging. It is obvious that the DISC structure has more practical value than conventional coil structures. Future research should improve the proposed structure for better shielding effect and transmission efficiency.

ACKNOWLEDGMENT

This work was supported in part by the National Nature Science Foundation of China under Grant 11901188, in part by the Natural Science Foundation of Hunan Province under Grants 2019JJ60055 and 2022JJ30226, in part by the Outstanding Youth Project of Hunan Education Department under Grants 20B186 and 18A272.

REFERENCES

1. Popović-Gerber, J. and J. A. Oliver, "Power electronics enabling efficient energy usage: Energy savings potential and technological challenges," *IEEE Transactions on Power Electronics*, Vol. 27, No. 5, 2338–2353, May 2012.
2. Khan, M. A. R. and A. Ahmed, "Wireless power transfer: An application to cell phone battery recharging," *2012 15th International Conference on Computer and Information Technology (ICCIT)*, 305–309, Dec. 2012.
3. Li, X. and C.-Y. Tsui, "A 13.56 MHz wireless power transfer system with reconfigurable resonant regulating rectifier and wireless power control for implantable medical devices," *IEEE Journal of Solid-State Circuits*, Vol. 50, No. 4, 978–989, Apr. 2015.

4. Choi, S. Y. and B. W. Gu, "Advances in wireless power transfer systems for roadway-powered electric vehicles," *IEEE Journal of Emerging and Selected Topics in Power Electronics*, Vol. 3, No. 1, 18–36, Mar. 2015.
5. Zhang, Y. and S. Chen, "Design of high-power static wireless power transfer via magnetic induction: An overview," *CPSS Transactions on Power Electronics and Applications*, Vol. 6, No. 4, 281–297, Dec. 2021.
6. Zheng, J. and G. Wei, "New development of electromagnetic compatibility in the future: Cognitive electromagnetic environment adaptation," *2021 13th Global Symposium on Millimeter-Waves & Terahertz (GSMM)*, 1–3, May 2021.
7. Mohammad, M. and M. S. Haque, "A litz-wire based passive shield design to limit EMF emission from wireless charging system," *2018 IEEE Energy Conversion Congress and Exposition (ECCE)*, 97–104, Sep. 2018.
8. Campi, T. and S. Cruciani, "Magnetic field mitigation by multicoil active shielding in electric vehicles equipped with wireless power charging system," *IEEE Transactions on Electromagnetic Compatibility*, Vol. 62, No. 4, 1398–1405, Aug. 2020.
9. Talluri, G. and M. Bindi, "Analysis of power losses due to magnetic shielding for electric vehicle wireless charging," *2021 IEEE 15th International Conference on Compatibility, Power Electronics and Power Engineering (CPE-POWERENG)*, 1–6, Jul. 2021.
10. Muramatsu, K. and Y. Gao, "Effect of eddy currents on method for evaluating shielding performance of magnetically shielded rooms using exciting coil," *IEEE Transactions on Magnetics*, Vol. 50, No. 11, 1–4, Nov. 2014.
11. Mohammad, M. and S. Choi, "Loss minimization design of ferrite core in a DD-coil-based high-power wireless charging system for electrical vehicle application," *IEEE Transactions on Transportation Electrification*, Vol. 5, No. 4, 957–967, Dec. 2019.
12. Li, J. and F. Yin, "Transmission efficiency of different shielding structures in wireless power transfer systems for electric vehicles," *CSEE Journal of Power and Energy Systems*, Vol. 7, No. 6, 1247–1255, Nov. 2021.
13. Choi, S. Y. and B. W. Gu, "Generalized active EMF cancel methods for wireless electric vehicles," *IEEE Transactions on Power Electronics*, Vol. 29, No. 11, 5770–5783, Nov. 2014.
14. Park, J. and D. Kim, "A resonant reactive shielding for planar wireless power transfer system in smartphone application," *IEEE Transactions on Electromagnetic Compatibility*, Vol. 59, No. 2, 695–703, Apr. 2017
15. Cruciani, S. and T. Campi, "Active shielding design for a dynamic wireless power transfer system," *2020 International Symposium on Electromagnetic Compatibility — EMC EUROPE*, 1–4, Sep. 2020.
16. Meng, J. and Y. Zhang, "Research of active magnetic shielding for wireless power transfer system of electric vehicles," *Advanced Technology of Electrical Engineering and Energy*, Vol. 40, No. 04, 44–51, Apr. 2021.
17. Narusue, Y. and Y. Kawahara, "Cancellation mechanism of electromagnetic leakage for wireless power transmission system based on magnetic resonant coupling," *2014 Asia-Pacific Microwave Conference*, 677–679, Nov. 2014.
18. Zhou, G., "Research on magnetic radiation suppression method of coupling mechanism of electric vehicle wireless power transmission system," Chongqing University, Chongqing, China, 2017.
19. Xu, J., "Research on electromagnetic compatibility of n-type magnetic coupling mechanism for dynamic wireless power supply of electric vehicles," Harbin Institute of Technology, Harbin, China, 2017.
20. Idris Elnait, K. E. and L. Huang, "Resonant reactive current shield design in WPT systems for charging EVs," *2018 IEEE PES Asia-Pacific Power and Energy Engineering Conference (APPEEC)*, 56–59, Oct. 2018.
21. Moon, H. and S. Kim, "Design of a resonant reactive shield with double coils and a phase shifter for wireless charging of electric vehicles," *IEEE Transactions on Magnetics*, Vol. 51, No. 3, 1–4, Mar. 2015.

22. Campi, T. and S. Cruciani, "Active coil system for magnetic field reduction in an automotive wireless power transfer system," *2019 IEEE International Symposium on Electromagnetic Compatibility, Signal & Power Integrity (EMC+SIPI)*, 189–192, Jul. 2019.
23. GB/T 38775-4, "Electric vehicle wireless power transfer — Part 4: Limits and test methods of electromagnetic environment," China Electricity Council, Beijing, China, 2020.
24. ICNIRP, "Guidelines for limiting exposure to time-varying electric and magnetic field (1 Hz to 100 kHz)," *Health Physics*, Vol. 99, No. 6, 818–836, 2010.